ARL-TR-8983 ● JUNE 2020

DEVCOM ARMY RESEARCH LABORATORY

An Exploding-Wire Circuit Model

by Paul R Berning and Matthew J Coppinger

NOTICES

Disclaimers

The findings in this report are not to be construed as an official Department of the Army position unless so designated by other authorized documents.

Citation of manufacturer's or trade names does not constitute an official endorsement or approval of the use thereof.

Destroy this report when it is no longer needed. Do not return it to the originator.

ARL-TR-8983 ● JUNE 2020

An Exploding-Wire Circuit Model

Paul R Berning and Matthew J Coppinger
Weapons and Materials Research Directorate, CCDC Army Research Laboratory

REPORT DOCUMENTATION PAGE

Form Approved
OMB No. 0704-0188

1. REPORT DATE *(DD-MM-YYYY)*	2. REPORT TYPE	3. DATES COVERED (From - To)
June 2020	Technical Report	1 May 2019–8 June 2020

4. TITLE AND SUBTITLE
An Exploding-Wire Circuit Model

5a. CONTRACT NUMBER

5b. GRANT NUMBER

5c. PROGRAM ELEMENT NUMBER

6. AUTHOR(S)
Paul R Berning and Matthew J Coppinger

5d. PROJECT NUMBER
AH80

5e. TASK NUMBER

5f. WORK UNIT NUMBER

7. PERFORMING ORGANIZATION NAME(S) AND ADDRESS(ES)
CCDC Army Research Laboratory
ATTN: FCDD-RLW-PA
Aberdeen Proving Ground, MD 21005

8. PERFORMING ORGANIZATION REPORT NUMBER
ARL-TR-8983

9. SPONSORING/MONITORING AGENCY NAME(S) AND ADDRESS(ES)

10. SPONSOR/MONITOR'S ACRONYM(S)

11. SPONSOR/MONITOR'S REPORT NUMBER(S)

12. DISTRIBUTION/AVAILABILITY STATEMENT
Approved for public release; distribution is unlimited.

13. SUPPLEMENTARY NOTES
ORCID ID: Paul R Berning, 0000-0001-9699-0245

14. ABSTRACT
A circuit model was developed to aid in predicting the outcome of exploding-wire experiments and to analyze the results of such experiments. The model tracks the internal energy of the wire over time and uses that to determine the temperature and resistance of the wire at each time step based on published heat capacity and resistivity values. A constant wire geometry is assumed. Individual models for pure magnesium, aluminum, titanium, copper, molybdenum, and tungsten wires were developed.

15. SUBJECT TERMS
exploding wire, circuit model, thermophysical properties, magnetic instabilities, pulsed power

16. SECURITY CLASSIFICATION OF:			17. LIMITATION OF ABSTRACT	18. NUMBER OF PAGES	19a. NAME OF RESPONSIBLE PERSON
a. REPORT	b. ABSTRACT	c. THIS PAGE			Paul R Berning
Unclassified	Unclassified	Unclassified	UU	46	19b. TELEPHONE NUMBER (Include area code) (410) 278-4509

Contents

List of Figures

List of Tables

Acknowledgments

The authors thank Jeffrey Ball, Keith Mahan, Robert Borys Jr, Colby Adams, and Brian Wilmer for their assistance in setting up and performing the exploding-wire experiment. They also thank Peter Bartkowski for reviewing the manuscript.

1. Introduction

This work is meant to support a program in which exploding-wire simulations generated by the hydrocode ALEGRA[1,2] are to be compared with the results of actual experiments. The goal of this work is to develop a model that couples key thermophysical effects with an inductance–resistance–capacitance (LRC) circuit model to aid in estimating the ultimate effect that a particular pulse will have on a wire, and to aid in extracting key experimental parameters from experimental data. This work is similar to the effort by Tucker and Toth,[3] though the methodology here is different and the goals are more limited.

Tucker and Toth's circuit model is a simple analytical model that envisions a uniform heating process with uniform phase changes, and predictable resistance increases, such that the entire heating process could be described by a simple 1-D semi-empirical model. While they were able to successfully mimic the results of their own exploding-bridge-wire (EBW) detonator experiments, their model proved to be less generalized than they had hoped. In the intervening years it has been shown that their model does not always give good quantitative results when applied to other experimental setups.[4,5]

The problem with Tucker's and Toth's methodology is that the process of exploding a wire electrically is much more complex than they envisioned. Complications can arise that make it nearly impossible to heat the wire uniformly. There is no simple 1-D or 2-D thermodynamic calculation that can accommodate these complications, hence the need for a more-complex code such as ALEGRA.

1.1 Complicating Effects

Consider the case of an isolated, infinitely long, perfectly smooth metal wire of constant cross section. When an electrical pulse is introduced to the wire, the current first sets up on the surface of the wire, due to the skin depth effect,[6] then diffuses inward toward the centerline as the pulse evolves. Thus the wire is heated from the outside to the inside, along its entire length, uniformly. The wire's surface melts, then vaporizes. As it is being converted to vapor, the resistance of the wire rises dramatically. Then, if enough energy is available, the vapor converts to plasma, an arc is formed, and the resistance drops dramatically. In EBW parlance, the time associated with the peak in resistance is referred to as "time of burst", and the stage at which an arc is formed and the current recovers is called "restrike".[3–5] This simple picture is precisely what Tucker and Toth envisioned, and their goal was to successfully predict such things as the time of burst and the peak resistance in a variety of situations.

This idealized picture is notable in that there are no magnetic forces acting on the wire. Even if the current densities and surface fields are large, at no point on the wire is the current coupled to the magnetic field that it generates because the current flows in a perfectly straight line. This assumption proves to be the problematic one, as there is nothing "perfect" about real-world wires. They may have inclusions, twists, bends, kinks, notches, or necked-down regions. Even if the defects are microscopic, they can still give rise to significant thermal and magnetic instabilities because the surface-current densities and the surface-field magnitudes can be enormous. The effects often come with a positive feedback mechanism and, as a rule, act to make the "defect" worse, which is why they are referred to as "instabilities". Cases where current is forced to flow around a bend or corner are particularly problematic; we refer to such cases as "kink instabilities".

Consider the case of a small, subtly necked-down (or notched) region on the surface of an otherwise smooth wire. The current must follow the surface, which means that it must briefly take an "inside corner" path. Since current tends to concentrate at inside corners (due to the precepts of magnetic induction), this sets up a hot spot at the bottom of the trough, which can lead to a localized thermal instability. Furthermore, the fact that the two sides of the trough are angled relative to each other means that they are magnetically coupled, resulting in a force that acts to deepen the trough. As this necked-down section is being pinched off, it is also being heated and softened, and since the heating rate at any given location is inversely proportional to the diameter raised to the fourth power it becomes a runaway process, and the necked-down section ends up vaporizing well in advance of the neighboring wire sections.

This type of magnetohydrodynamic (MHD) instability is sometimes referred to as a "sausage instability" (not to be confused with the mechanical instability of the same name), as it tends to occur at a series of points along the wire, resulting in a series of isolated wire sections arrayed like a string of sausages.[7] The effect greatly complicates the electrification process because the vapor clouds that form where the necked-down sections were can quickly expand and envelop the intervening wire sections, at which point some of the current can bypass those sections entirely. In short, the effects that accompany rapid electrical heating make it virtually impossible to heat the wire uniformly along its length. They can also make it difficult to vaporize all parts of the wire. Unsurprisingly, there is no simple method of incorporating this behavior in a circuit model, as it is highly situation-dependent. This is the type of complication that Tucker and Toth[3] did not account for, and the reason that ALEGRA is necessary.

The "sausage instability" is most obvious in extreme cases where macroscopic defects are intentionally introduced in the conductor, as in the segmented rod

experiments described in Hollandsworth et al.[8] In those experiments, large currents were introduced into brass rods that had a series of necked-down sections machined into them. It was shown that the necked-down sections would quickly vaporize but the thicker sections between them would remain intact for the duration of the pulse, having been protected from the electrical current by the enveloping vapor clouds. Encasing the segmented rod in an insulating tube resulted in the entire rod being destroyed, as the vapor clouds were constrained in that case.

1.2 Example

The pulses that will be used in the planned exploding-wire experiments are of the "slow" type,[9] in that the initial risetime of the current pulse is measured in kiloamperes/microsecond rather than kiloamperes/nanosecond. In experiments like this the first evidence of "kink instabilities" that often appears is the ends of the wire blowing off at the connection points. This occurs because the end-connection-to-wire junctions are often the largest "kinks" in the current path.

In the main section of the wire the MHD and thermal instabilities are seeded by microscopic defects and are thus slower to appear. What results is typically an alternating series of narrow liquefied sections separated by narrow vaporized sections. In a flash X-ray radiograph the wire takes on a "striped" appearance (as only the liquid sections are visible). Historically, these stripes have been referred to as "striations".[9] Thus, only a series of localized wire sections actually explode rather than the entire wire. Since the liquefied and vaporized sections alternate along the axis of the wire, the high-resistance metal vapor begins to restrict current well before the wire is completely vaporized, hence "burst" does not coincide with full vaporization. To complicate matters further, shortly after striations form, the individual vapor clouds expand and form a continuous sheath around the liquefied sections, offering a parallel path that allows some of the current to bypass the liquefied sections entirely. Plasma formation then follows.

The intervening liquid sections (i.e., striations) flatten axially and expand radially as time goes on, largely as an inertial response to the impact of the explosions occurring on both sides of them. In cases where the interaction between the expanding vapor clouds and liquid droplet are particularly symmetric, the striation is just a liquid-mist smoke ring viewed from the side.

All of these effects are illustrated in Fig. 1, which contains 150-kV flash X-ray radiographs associated with a series of identical exploding copper (Cu) wire experiments that are described in Zellner et al.[10] Each image is taken at a different time in the process. The first image on the left shows a narrow section of wire in its pristine state. The next image shows that section of wire with its ends blown off

and with striations already apparent. The subsequent images show the striations expanding (note that the third image from the left shows at least one clear smoke ring).

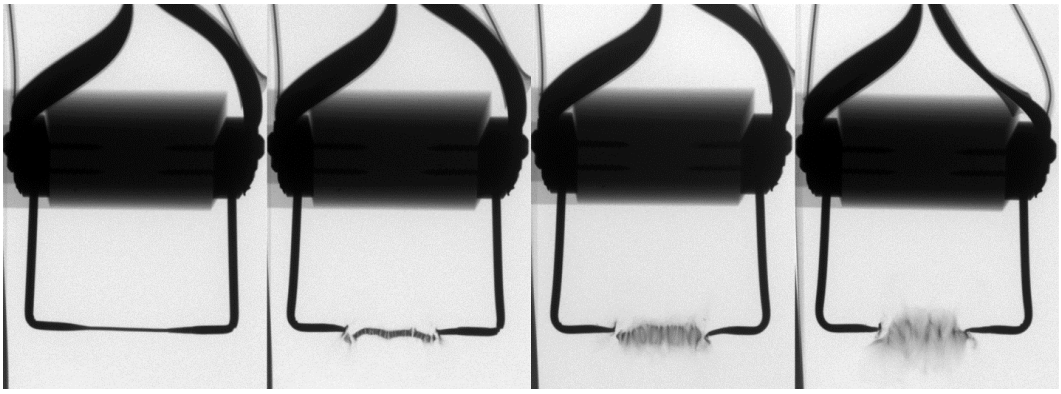

Fig. 1 X-ray radiographs associated with a series of three identical exploding-wire experiments. Each image was taken at a different time in the process.[10]

High-speed videos of these experiments were obtained using a Shimadzu model HPV-X2 framing camera operating at a 5-MHz frame rate. Figure 2 contains the frames that correspond with the times that the last three radiographs in Fig. 1 were taken. The main takeaway is that the entire gap was filled with Cu plasma almost immediately. That offers the current a lower inductance path than the relatively narrow, discontinuous liquid-mist channel, which may be why the striations persist so long. In the images, the two large, bright vapor (or plasma) clouds emanating from the blown-off wire ends are the most obvious feature, though a wide vapor channel emanating from the central portion of the wire is also evident.

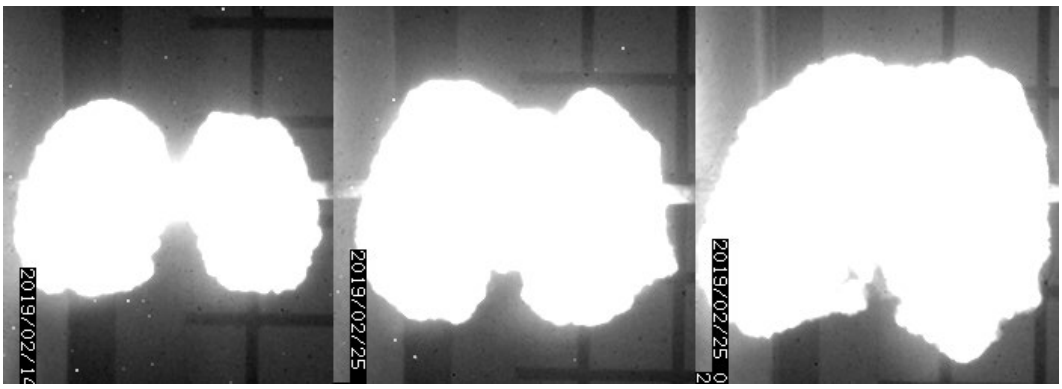

Fig. 2 High-speed video frames corresponding to the last three flash X-ray radiographs seen in Fig. 1, showing a magnified view section of wire that explodes[10]

The goal of this work is to develop a circuit model that couples the basic LRC circuit equations with zero-dimensional thermodynamic calculations that track the effect of heating on the heat capacity and resistance of the wire. As there is no way to include the complicated effects of localized heating in such a calculation, the model's specific predictions will likely only be valid up to the point where boiling begins, which may be a very short time into the process. That may be sufficient to aid in measuring the parasitic inductance and parasitic resistance of the system, key parameters that will be required for subsequent ALEGRA modeling. Beyond that, the model is only expected to give a general idea of how much heating will occur and when key events will occur and thus aid in planning.

2. Circuit Model Description

Tucker, in Tucker and Toth,[3] concluded that the quantity that determined when burst would occur in an EBW, independent of what fireset was used (i.e., what power supply was used or what pulse shape was supplied), was "action until burst", defined by

$$A = \int_0^{t_b} I^2(t)dt \tag{1}$$

where t is time, t_b is the time of burst, and I is the measured current. Consequently, Tucker's and Toth's model tracked all key material parameters in time according to what level of action had been achieved at that time. They assumed that the resistivity of each phase of the material varied linearly with temperature, and they associated burst with the vaporization of the entire wire. They also made an effort to simulate the onset of plasma formation.

However, since then it has been shown that the "action until burst" is not a universal metric that decides when burst will occur and that the Tucker–Toth model did not work effectively for all firesets, in part because the events that occur at burst are more complicated than they envisioned.[4,5]

In this work, as in Valancius et al.,[4] we track specific enthalpy (i.e., energy density) rather than action, and, unlike Tucker, we use published values of heat capacity and resistivity to associate this metric with temperature and resistance rather than fitted values. Furthermore, we make no attempt to recreate the situation beyond the onset of vaporization, as events become complex and situation-dependent at about that time.

2.1 Heat Capacity Data

Models were developed for magnesium (Mg), aluminum (Al), titanium (Ti), Cu, molybdenum (Mo), and tungsten (W) wires. In each case, information regarding the temperature dependence of the heat capacities of the materials was acquired, as were other key thermophysical parameters such as specific heat of fusion and specific heat of vaporization. In all cases except the W case, this information came from the National Institute of Standards (NIST) Chemistry WebBook,[11] which in turn gets its information from Chase[12] and Cox et al.[13]

In most cases the heat capacity data compiled in Chase[12] and Cox et al.[13] were last reviewed in either the 1970s or 1980s. One exception is W data, which were last reviewed in the 1960s. Given that the melting and boiling points of W are extremely high, and that the most appropriate method for measuring the high-temperature thermophysical properties of refractory metals (i.e., microsecond pulsed heating)[14] was developed in the 1970s, we rely on a more modern review by Tolias et al.[15] in that case.

NIST WebBook[11] heat-capacity values are presented as a fit of existing data to the Shomate equation. Using NIST's notation, this equation takes the form

$$C_p° = A + B\tau + C\tau^2 + D\tau^3 + E/\tau^2 \quad (2)$$

where $C_p°$ = heat capacity (in J/mol*K), τ = temperature (kelvin)/1,000, and the constants A, B, C, D, and E are fitted parameters. NIST also supplies parameters to calculate related quantities:

$$H°-H°_{298.15} = A\tau + B*\tau^2/2 + C*\tau^3/3 + D\tau^4/4 - E/\tau + F - H \quad (3)$$

$$S° = A*ln(\tau) + B\tau + C\tau^2/2 + D\tau^3/3 - E/(2\tau^2) + G \quad (4)$$

where $H°$ = standard enthalpy (in kJ/mol) and $S°$ = standard entropy (in J/mol*K) and the constants F, G, and H are fitted parameters.

In this work we will omit the superscript "o" when referring to C_p and simply refer to the enthalpy increase starting at room temperature as "ΔH".

The circuit model assigns a wire temperature at each point in time on the basis of the level of specific enthalpy achieved at that point in time using a lookup table. In each case the lookup table is generated from polynomial fits to the specific enthalpy (ΔH) versus temperature (T) curves associated with each phase (solid, liquid, and gas) of the metal in question. Polynomial fits were used because they provide a relatively simple functional form for the lookup table that is directly applicable to

the circuit model in this study. The fitted polynomial coefficients will be listed in following sections of this report. First- and second-order polynomial fits proved to be sufficient in most cases, with key features such as latent heat of fusion and vaporization recreated to within approximately 1%. The one exception was solid Mo, where a third-order polynomial was required to achieve that level of accuracy.

2.2 Resistivity Data

Resistivity (ρ) versus temperature (T) data were obtained from published sources. The quality and reliability of the data varies from metal to metal. Some metals have been studied extensively over the entire temperature range of interest; the data extensively reviewed and recommended values supplied. Other metals have not been studied extensively, or there is little agreement in the data sets, or there is very little high-temperature data available. In some cases the high-temperature data are taken from a single experiment because that is all that is available.

The sources used are described in the individual sections that follow. Cases where resistivity is well characterized—Cu, Al, Mo, and W—are presented first. Cases where resistivity data are somewhat questionable—Ti and Mg—follow. Unlike Tucker, who assumed a linear dependency,[3] we fit each resistivity versus temperature curve to quadratic polynomials so that a lookup table of ρ versus T values can be generated for use by the circuit model. With the exception of the Mg data, all referenced resistivity values are corrected for thermal expansion.

2.3 Circuit Model

In exploding-wire experiments, the circuit generally consists of a high-voltage capacitor, a high-voltage switch, the wire that acts a load, and the hardware necessary to connect the circuit elements together. The relevant circuit model is that of a series *LRC* circuit (where L is lumped inductance, R is lumped resistance, a C is lumped capacitance). Applying Kirchhoff's law to that circuit yields the governing differential equation:

$$0 = \frac{Q}{C} + R\frac{dQ}{dt} + \frac{d}{dt}\left(L\frac{dQ}{dt}\right) \tag{5}$$

where Q is the charge on the capacitor and t is time. This equation is numerically integrated to solve for current as a function of time, as defined by

$$I(t) = -\frac{dQ}{dt} \tag{6}$$

In the simplest case, R, L, and C are all constant. In this analysis, R is allowed to vary with temperature. To assign a particular temperature to the wire at each time step, the specific enthalpy achieved by that time must be calculated so that the ΔH versus T lookup table can be referenced. As the only heat source is ohmic, the specific enthalpy achieved at any time (starting at room temperature) is given by

$$\Delta H(t) = \frac{1}{m}\int_0^t R_{wire}\,(t)\,I(t)^2\,dt \tag{7}$$

where m is the mass of the wire, and $R_{wire}(t)$ is the resistance of the wire at any given time. Once ΔH is calculated, the corresponding temperature is found in the lookup table and assigned to the next time step. Any temperature-dependent variables will then change accordingly.

In this model it is assumed that the wire retains its initial geometry throughout, which is to say that the model does not account for the effect. Skin-depth effects are also ignored. Given those two assumptions, the resistance of the wire at any given time is calculated by finding the appropriate resistivity in the ρ versus T lookup table and applying the equation:

$$R_{wire} = \rho(T) * (\frac{l}{\pi r^2}) \tag{8}$$

where l is the length of the wire and r is the radius of the wire.

As the resistivity of metals tend to increase when a phase change occurs, a method must be developed to track the change in resistance as the phase change is occurring. Here we are primarily concerned with the melting event. Tucker and Toth[3] assumed a radial melting mode, such that the solid and liquid portions act like resistors in parallel throughout the melting event. If ρ_1 is the resistivity of the solid phase at the melt temperature, ρ_2 is the resistivity of the liquid phase at the melt temperature, H_{fus} is the specific heat of fusion, and ε is the specific energy in the wire above and beyond that needed to reach the melting point, then it can be shown that the effective resistivity of the wire during the melt phase is given by

$$\rho(\varepsilon) = \frac{\rho_1}{1-\left(\frac{\rho_2-\rho_1}{\rho_2}\right)\frac{\varepsilon}{H_{fus}}} \tag{9}$$

As pointed out by Tucker and Toth,[3] this function is concave upward. Alternately, if one assumes that melting mode is NOT radial in nature, but rather that localized instabilities create a series of alternating solid and liquid wire segments, then the liquid and solid portions act like resistors in series, and it can be shown that the effective resistivity of the wire is given by

$$\rho(\varepsilon) = \rho_1 + (\rho_2 - \rho_1)\frac{\varepsilon}{H_{fus}} \quad (10)$$

This equation is equivalent to linear interpolation between the values of ρ_1 and ρ_2 and is the default choice in this model. Modeling indicates that the choice of equation has little effect on the shape of the current pulse and only a modest effect on the voltage trace in most cases of interest here. In cases where the values of ρ_1 and ρ_2 are similar (e.g., Mo, W, and Ti), it matters even less.

While Tucker and Toth attempted to mimic the resistance changes during vaporization and plasma formation, in this model we simply assume the vapor phase resistivity continues to follow the liquid-phase trend, and thus no interpolation is required during that phase change. This probably understates the resistance increase associated with this phase change. As stated earlier, there is no way to faithfully simulate this transition in a simple circuit model.

Given a constant wire geometry, the inductance of the wire L_{wire} also remains constant. The value of L_{wire} is assumed to be given by Grover[16]:

$$L_{wire} = 2l\left\{ln\left[\frac{l}{r}\left(1+\sqrt{1+\left(\frac{r}{l}\right)^2}\right)\right] - \sqrt{1+\left(\frac{r}{l}\right)^2} + \frac{r}{l} + \frac{\mu}{4}\right\} \quad (11)$$

where L_{wire} is inductance of the wire in nanohenries (nH), l is the wire length in centimeters, r is the wire radius in centimeters, and μ is the magnetic permeability of the material ($\mu = 1$ in all cases discussed here).

In the exploding-wire circuit in question, the only appreciable source of capacitance is the capacitor, so the value of C is easy to determine. This is not the case when it comes to L and R; in those cases the parasitic inductance and resistance of the capacitor bank and interconnections cannot be ignored. Thus, we treat R and L as coming from two sources:

$$L = L_{wire} + L_{parasitic} \quad (12)$$

and

$$R = R_{wire} + R_{parasitic} \quad (13)$$

where the values of $L_{parasitic}$ and $R_{parasitic}$ are not obvious and usually difficult to calculate from first principles. It is often easier to extract those values from an analysis of the circuit's current trace, which is one of the goals of this work.

2.4 Example

The results of an actual exploding-wire experiment are now compared with the predictions of the circuit model (the thermophysical property inputs for Cu are described in the following section). The exploding-wire experiment in question involved a pure Cu wire 1.59 mm in diameter and 91.0 mm long. It was held in a fixture that was designed to apply the current to the ends of the wire in an axisymmetric fashion. The capacitor bank that supplied the electrical energy had a nominal capacitance of 1,400 μF. It was charged to 6.0 kV initially, representing 25.2 kJ of stored energy. Current flow was initiated by a spark gap switch. Current data were obtained by numerically integrating the output of a calibrated Rogowski coil. Voltage data was obtained by a pair of high-voltage probes attached to the two ends of the fixture holding the wire.

Figure 3 contains a plot of the measured current in the wire versus time compared with the "best fit" obtained using the circuit model. The fit assumes that the capacitance is 1,400 μF, the parasitic resistance was 6.4 mΩ, and the parasitic inductance was 328 nH. The wire's inductance was calculated to be 85.4 nH, and its initial resistance at room temperature was calculated to be 0.788 mΩ.

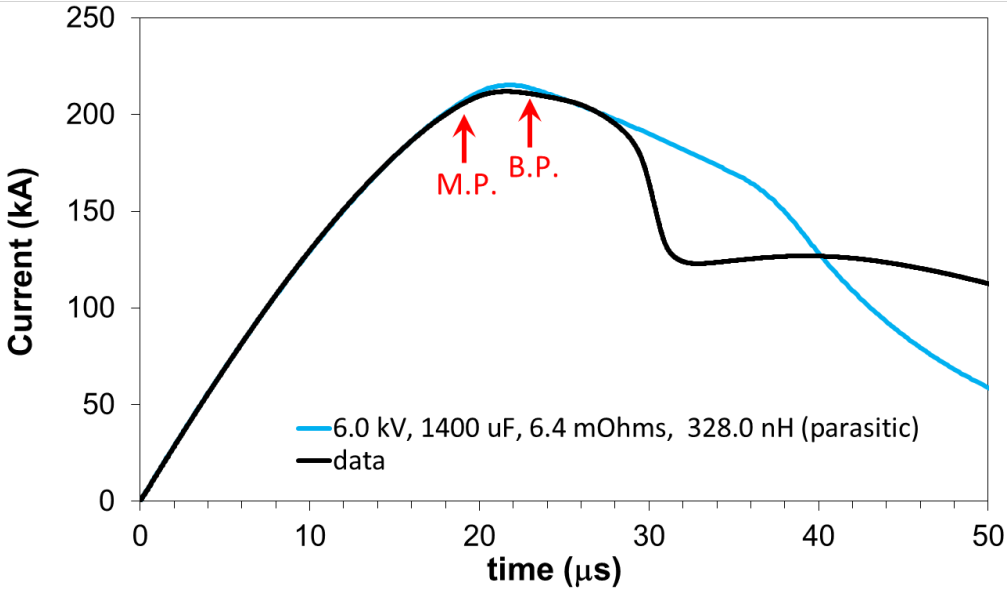

Fig. 3 Current data from an exploding-wire experiment compared with results of the circuit model

The times at which the melting point and boiling points are attained (as determined by the simplified circuit model) are marked in Fig. 3. As expected, the model becomes untenable a short while after the boiling point is reached due to instability effects not included in the model. In the fit, the parasitic inductance is largely determined by the rate of rise near t = 0. The parasitic resistance is largely determined by the shape of the peak. This is demonstrated in Fig. 4, which illustrates the effects of varying the assumed parasitic resistance.

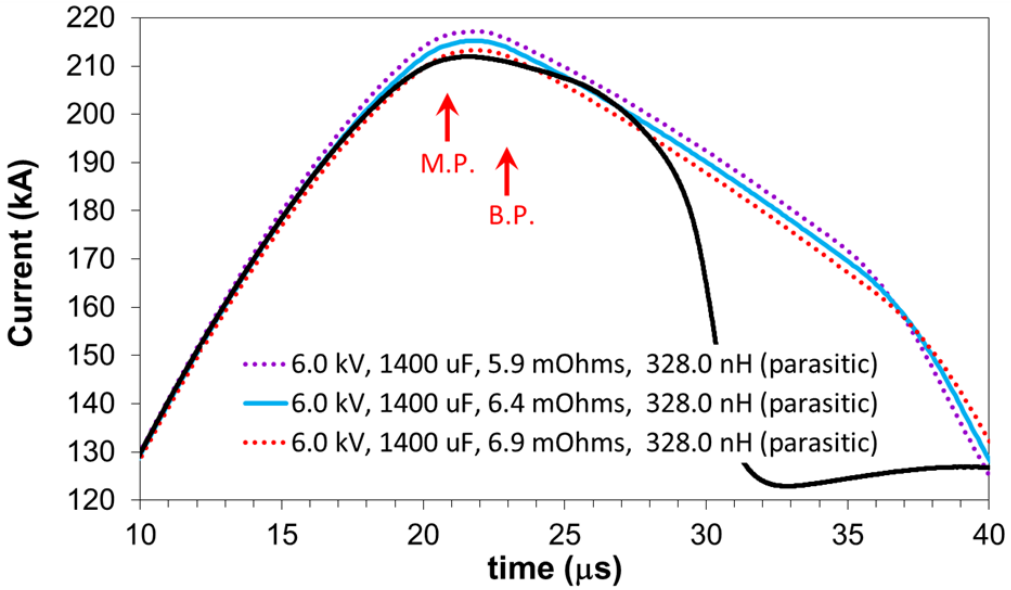

Fig. 4 Effect of varying the assumed parasitic resistance in the circuit model

The voltage-difference data obtained from this experiment are plotted in Fig. 5. The data have been smoothed to reduce the high-frequency noise seen near t = 0, which comes from the spark gap switch. Since the high-voltage probes were attached to the wire mounting fixture rather than the wire itself, the signal includes the effects of resistance of the wire, the resistance in the mount (assumed to be negligible), and the inductance of the wire and mount combination. In this case, the value of L_{mount} is estimated to be 29.6 nH, such that $L_{wire} + L_{mount} = 115$ nH, based on the signal level at t = 0.

The model predicts that the melting point is achieved at 19.6 μs, full melt at 20.8 μs, boiling point at 22.9 μs, and full vaporization at 35.2 μs.

As expected, the model performs reasonably up to a point just after the theoretical boiling point is achieved. After that, instabilities take over and burst occurs before the predicted point of full vaporization. The fact that the voltage level obtained at burst is much larger than the peak predicted by the model indicates that the model's assumption that the resistivity of the vapor follows the trends set by the liquid is naïve. Copper vapor would appear to have a much higher resistivity than that.

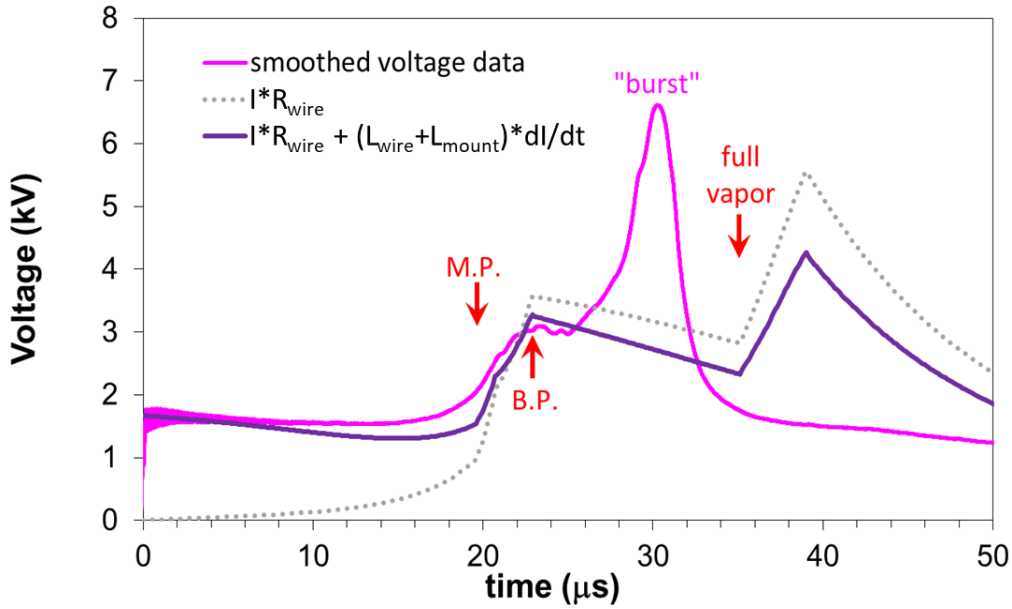

Fig. 5 Voltage data from the exploding-wire experiment compared with results of the circuit model

3. Copper Wires

In this work the melting point of Cu is taken to be 1,358 K, boiling point is 2,843 K, mass density is 8.96 g/cm^3, and atomic mass is 63.546.

3.1 Copper Heat Capacity

NIST's Shomate fit parameters for pure Cu are listed in Table 1. They yield C_p in J/mol*K and $H°$ in kJ/mol, as described in Eqs. 2 and 3. While the NIST WebBook[11] lists all such parameters to six significant figures, it does not imply that the underlying data are correct to that level of precision.

Table 1 Parameters that describe NIST's Shomate equation fits for pure Cu[12,13]

Parameter	Solid (298–1,358 K)	Liquid (1,358–2,843 K)	Gas (2,843–6,000 K)
A	1.77289E+01	3.28445E+01	–8.04864E+01
B	2.80987E+01	–8.40000E–05	4.93587E+01
C	–3.12529E+01	3.20000E–05	–7.57806E+00
D	1.39724E+01	–4.00000E–06	4.04960E–01
E	6.86110E–02	–2.80000E–05	1.33338E+02
F	–6.05659E+00	–1.80490E+00	5.19933E+02
G	4.78959E+01	7.39231E+01	1.93535E+02
H	0.00000E+00	1.18573E+01	3.37600E+02

Figure 6 contains a plots of C_p (in J/g*K) versus temperature based on the three Shomate equation fits described previously. Figure 7 contains a plot of the energy per gram needed to achieve various temperatures (i.e., ΔH in joules per gram), starting at room temperature, based on NIST's Shomate fits.

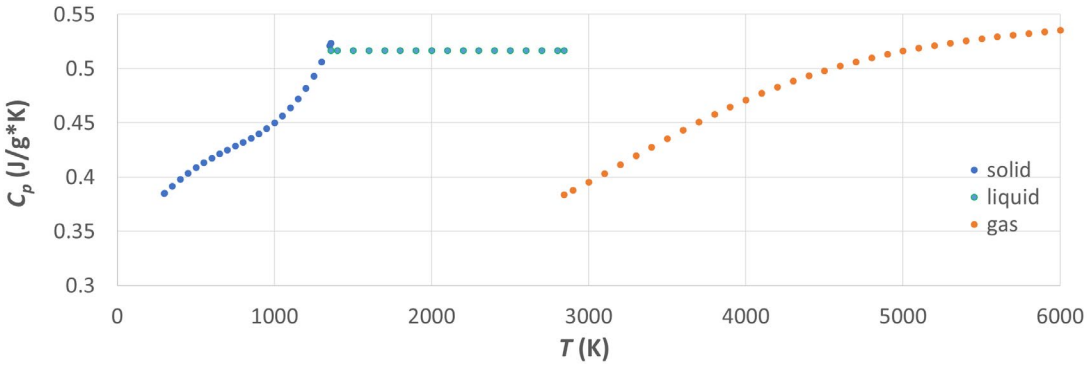

Fig. 6 Recommended values for heat capacity of Cu[12,13]

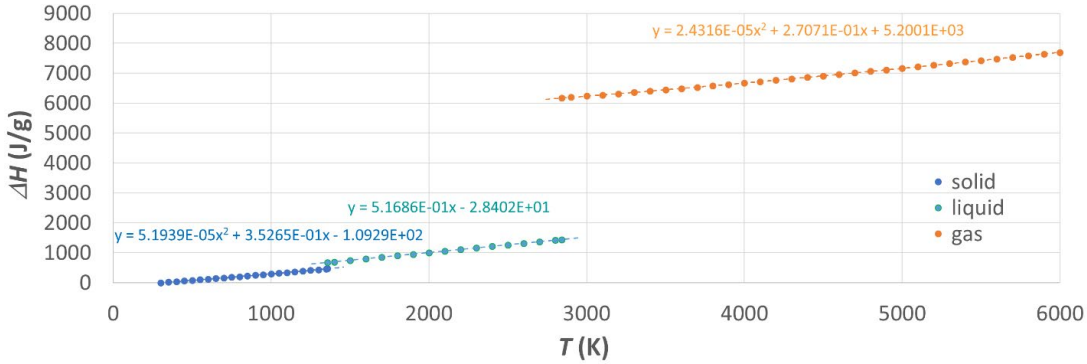

Fig. 7 Specific energy needed to raise Cu to various temperatures starting at room temperature

The three dashed lines seen in Fig. 7 represent polynomial fits to the three temperature intervals laid out in Table 1. They represent functions of the form $\Delta H = a + b*T + c*T^2$, where ΔH is in joules per gram and T is in kelvin. These polynomial fits are used to develop a lookup table that yields temperature as a function of of energy input (per gram). The fitted coefficients used for this are listed in Table 2.

Table 2 Parameters that describe polynomial fits to the curves in Fig. 7

Coefficient	Solid (298–1,358 K)	Liquid (1,358–2,843 K)	Gas (2,843–6,000 K)
a	–1.0929E+02	–2.8402E+01	5.2001E+03
b	3.5265E-01	5.1686E–01	2.7071E–01
c	5.1939E-05	…	2.4316E–05

The three polynomial fits seen in Fig. 7 can be used to calculate key quantities, such as the energy required to raise a mass of Cu from room temperature to the melting point, latent heat of fusion, energy required to raise the temperature from the melting point to the boiling point, and latent heat of vaporization. The numbers derived from the polynomial fits are compared with the numbers derived from the Shomate equation fits in Table 3. The largest disagreement is between the two latent heat of vaporization values, which differ by 1.4%.

Table 3 Key quantities derived from fits (Cu)

Quantity	Polynomial fits (J/g)	NIST Shomate fits (J/g)
Energy to heat from 298 to 1,358 K	464.98	466.88
Latent heat of fusion	208.51	206.62
Energy to heat from 1,358 to 2,843 K	767.54	767.54
Latent heat of vaporization	4,725.24	4,731.70

3.2 Copper Resistivity

Figure 8 contains values for the resistivity of both solid and liquid Cu recommended in the review by Matula[17] for temperatures between 250 and 1,700 K. Figure 8 also contains values of the resistivity of liquid Cu as measured by Gathers[18] for temperatures between the melting point and 3,500 K.

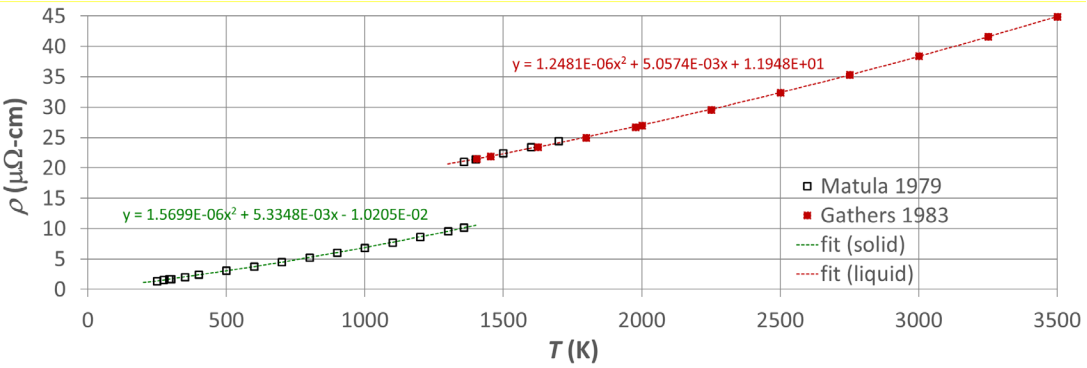

Fig. 8 Resistivity of pure Cu vs. temperature[18,19]

The dashed lines in Fig. 8 represent fits to quadratic polynomials of the form $\rho = d + e*T + f*T^2$, where ρ is resistivity in μΩ-cm and T is temperature in kelvin. In the case of solid Cu, Matula's[17] values were fitted. In the case of liquid Cu, Gathers'[18] values were fitted, as they are in excellent agreement with Matula's values and cover a wider range. The coefficients of the fitted polynomials are listed in Table 4. These fitted values are used to create a ρ versus T lookup table for use by the circuit model.

Table 4 Parameters that describe polynomial fits to the resistivity vs. temperature curves in Fig. 8

Coefficient	Solid (298–1,358 K)	Liquid (1,358–2,843 K)
d	–1.0205E–02	1.1948E+01
e	5.3348E–03	5.0574E–03
f	1.5699E–06	1.2481E–06

4. Aluminum Wires

In this work, the melting point of Al is taken to be 933 K, boiling point is 2,791 K, mass density is 4.506 g/cm^3, and atomic mass is 26.9815.

4.1 Aluminum Heat Capacity

Parameters for Shomate fits to Al data are listed in Table 4.1 of the NIST WebBook.[11] They yield C_p in J/mol*K and $H°$ in kJ/mol, as described in Eqs. 2 and 3, and are based on data last reviewed in 1983.[12,13]

Table 5 Parameters that describe NIST's Shomate equation fits for pure Al

Parameter	Solid (298–933 K)	Liquid (933–2,791 K)	Gas (2,791–6,000 K)
A	2.80892E+01	3.17510E+01	2.03769E+01
B	–5.41485E+00	3.93583E–08	6.60817E–01
C	8.56042E+00	–1.78652E–08	–3.13631E–01
D	3.42737E+00	2.69417E–09	4.51060E–02
E	–2.77375E–01	5.48004E–09	7.81730E–02
F	–9.14719E+00	–9.45684E–01	3.23858E+02
G	6.19098E+01	7.33995E+01	1.89481E+02
H	0.00000E+00	1.05620E+01	3.29699E+02

Figure 9 contains plots of C_p (in J/g*K) versus temperature based on the three fits described previously. Figure 10 contains a plot of the energy per gram needed to achieve various temperatures ΔH versus temperature based on these fits.

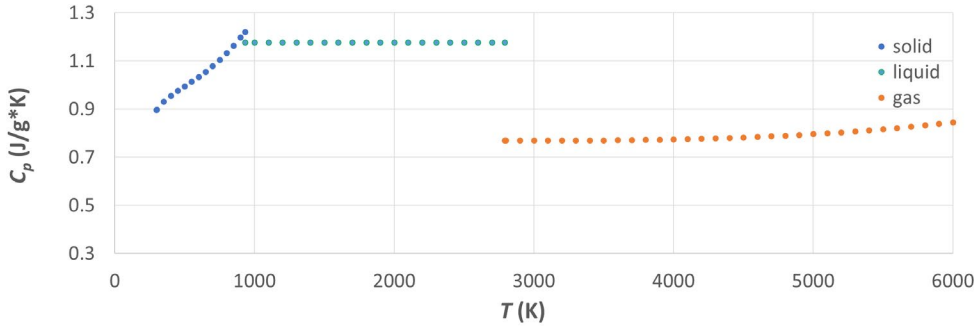

Fig. 9 Recommended values for heat capacity of Al[12,13]

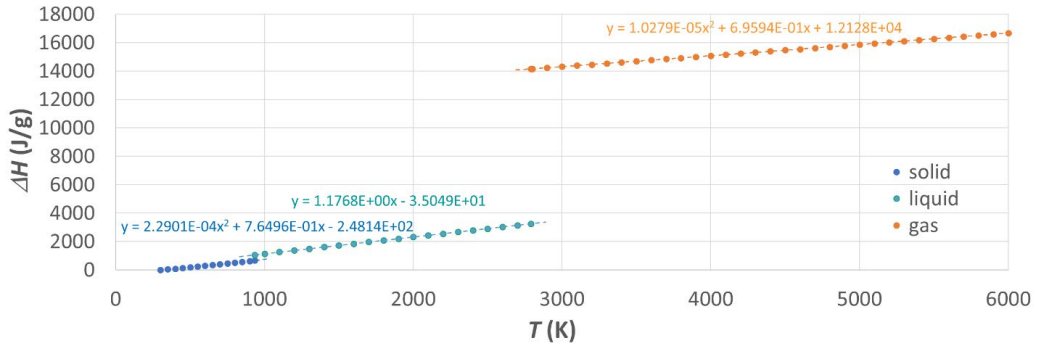

Fig. 10 Specific energy needed to raise Al to various temperatures starting at room temperature

The three dashed lines in Fig. 10 represent polynomial fits to the three temperature intervals laid out in Table 5. They represent functions of the form $\Delta H = a + b*T + c*T^2$, where ΔH is in joules per gram and T is in kelvin. These polynomial fits are used to develop a lookup table that yields temperature as a function of of energy input. The coefficients that describe these fits are listed in Table 6.

Table 6 Parameters that describe polynomial fits to the curves in Fig. 10

Coefficient	Solid (298–933 K)	Liquid (933–2,791 K)	Gas (2,791–6,000 K)
a	–2.4814E+02	–3.5049E+01	1.2128E+04
b	7.6496E–01	1.1768E+00	6.9594E–01
c	2.2901E–04	…	1.0279E–05

Key quantities were calculated using both the polynomial fits and the Shomate equation fits. These numbers are compared in Table 7. Agreement is better than 0.3% in all cases.

Table 7 Key quantities derived from fits (Al)

Quantity	Polynomial fits (J/g)	NIST Shomate fits (J/g)
Energy to heat from 298 to 933 K	664.76	665.91
Latent heat of fusion	398.15	396.96
Energy to heat from 933 to 2,791 K	2,186.5	2,186.4
Latent heat of vaporization	10,901	10,897

4.1 Aluminum Resistivity

Desai et al.[19] reviewed Al resistivity data and developed a list of recommended values up to a temperature of 2,000 K. These values are plotted in Fig. 11. In this work, the resistivity of solid Al is derived from a polynomial fit to Desai et al.'s recommended values.

Desai et al. decided that above 2,000 K the disparity between the available data sets was too great to develop reliable figures. Since Gathers' measurement[18] (up to 4,000 K, also plotted in Fig. 11) seems to agree well with Desai et al.'s values, a polynomial fit to Gathers' data is used to determine the resistivity of liquid Al.

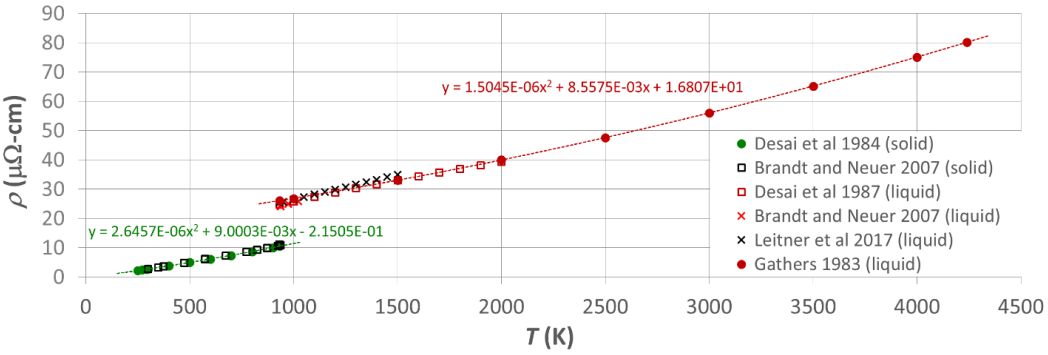

Fig. 11 Resistivity of pure Al vs. temperature[18–21]

The data were fitted to quadratic polynomials of the form $\rho = d + e*T + f*T^2$, where ρ is resistivity in μΩ-cm and T is temperature in kelvin, for the purpose of developing a lookup table that yields resistivity as a function of temperature. The coefficients of these polynomials are listed in Table 8.

Table 8 Parameters that describe polynomial fits to the curves in Fig. 11

Coefficient	Solid (298–933 K)	Liquid (933–2,791 K)
d	–2.15050E–1	1.68074E+1
e	9.00032E–3	8.55748E–3
f	2.64568E–6	1.50449E–06

5. Molybdenum Wires

In this work the melting point of Mo is taken to be 2,896 K, boiling point is 4,952 K, mass density is 10.28 g/cm^3, and atomic mass is 95.96.

5.1 Molybdenum Heat Capacity

Parameters for fits to Mo data are listed in Table 5 of the NIST WebBook.[11] They yield C_p in J/mol*K and $H°$ in kJ/mol, as described in Eqs. 2 and 3. They are based on data last reviewed in 1978.[13,14]

Table 9 Parameters that describe NIST's Shomate equation fits for pure Mo

Parameter	Solid (298–1,900 K)	Solid (1,900–2,896 K)	Liquid (2,896–4,952 K)	Gas (4,952–6,000 K)
A	2.47274E+01	1.23119E+03	3.76560E+01	6.79285E+01
B	3.96043E+00	–9.63425E+02	–7.18807E–08	–4.05370E+01
C	–1.27071E+00	2.83729E+02	1.41343E–08	1.16714E+01
D	1.15307E+00	–2.80410E+01	–9.52638E–10	–8.19432E–01
E	–1.70246E–01	–7.12204E+02	–1.56280E–07	–2.21404E+01
F	–8.11068E+00	–1.48553E+03	1.68155E+01	6.00822E+02
G	5.64338E+01	5.73785E+02	7.04816E+01	2.31671E+02
H	0.00000E+00	0.00000E+00	4.15680E+01	6.58980E+02

Figure 12 contains plots of C_p (in J/g*K) versus temperature based on the fits described previously. Figure 13 contains a plot of the specific energy needed to achieve various temperatures, ΔH versus temperature, based on these fits.

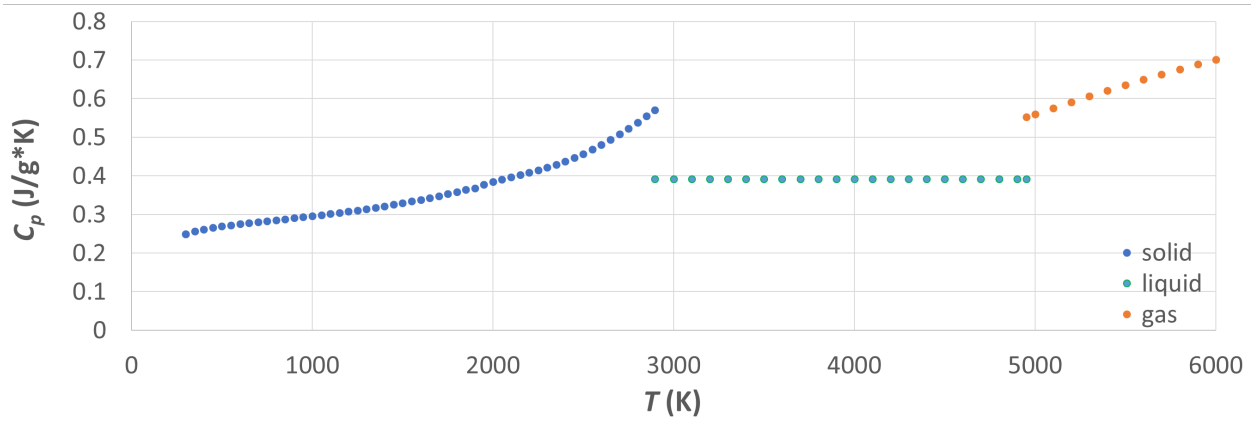

Fig. 12 Recommended values for the heat capacity of Mo[12,13]

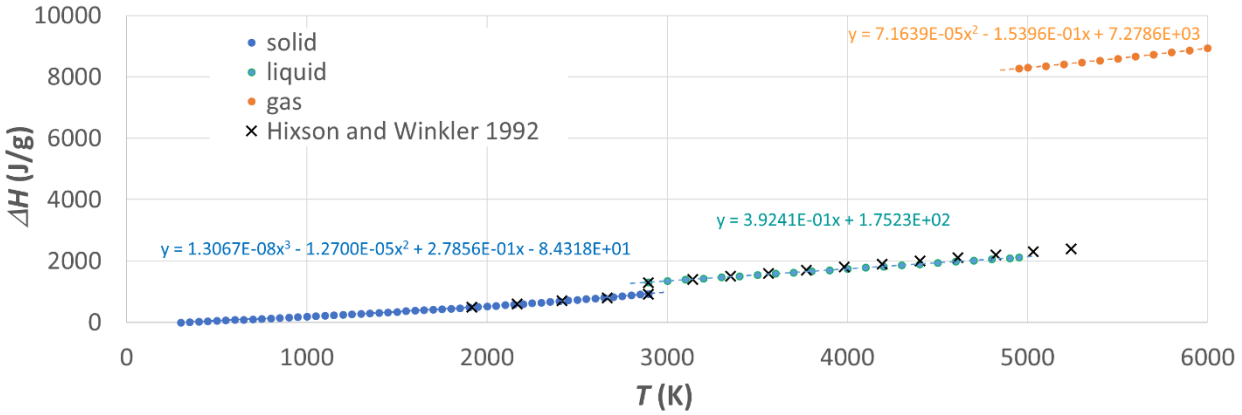

Fig. 13 Specific energy needed to raise Mo to various temperatures, starting at room temperature, according to the NIST WebBook.[11] Data from Hixson and Winkler[22] are plotted for comparison.

The dashed lines in Fig. 13 represent polynomial fits to the Shomate-derived values. The shape of the Mo solid-state enthalpy versus temperature curve was the only enthalpy curve not well fit by a second-order polynomial. In this case a third-order polynomial was used. Parameters for these fits are listed in Table 10. Data from an experiment that postdates the Shomate fits[22] are also plotted in Fig.13, showing good agreement with the recommended values.

Table 10 Parameters that describe polynomial fits to the curves in Fig. 13

Coefficient	Solid (298–2,896 K)	Liquid (2,896–4,952 K)	Gas (4,952–6,000 K)
a	–8.4318E+01	1.7523E+02	7.2786E+03
b	2.7856E–01	3.9241E–01	–1.5396E–01
c	–1.2700E–05	…	7.1639E–05
d	1.3067E–08	…	…

Once again, key quantities were calculated using both the polynomial fits and the Shomate equation fits. These numbers are compared in Table 11. Agreement is within 1% in all cases.

Table 11 Key quantities derived from fits (Mo)

Quantity	From polynomial fits (J/g)	NIST Shomate (J/g)
Energy to heat from 298 to 1,358 K	935.34	936.83
Latent heat of fusion	378.44	374.84
Energy to heat from 1,358 to 2,843 K	806.76	806.80
Latent heat of vaporization	6,154.55	6,154.68

5.2 Molybdenum Resistivity

Mo resistivity is well-characterized in the literature. Reviews for both solid and liquid Mo resistivity exist.[22,23] Recommended values from both reviews are plotted in Fig. 14. Recommended values for liquid Mo were supplied in equation form[23]:

$$\rho(T) = 97.10 + 7.9913 \times 10^{-3}(T - T_m) + 8.0148 \times 10^{-7}(T - T_m)^2 \qquad (14)$$

where ρ is measured in μΩ·cm, T is measured in kelvin, and T_m is the melting point temperature. More-recent data[22] are also plotted in Fig. 14. They are in excellent agreement with the recommended values.

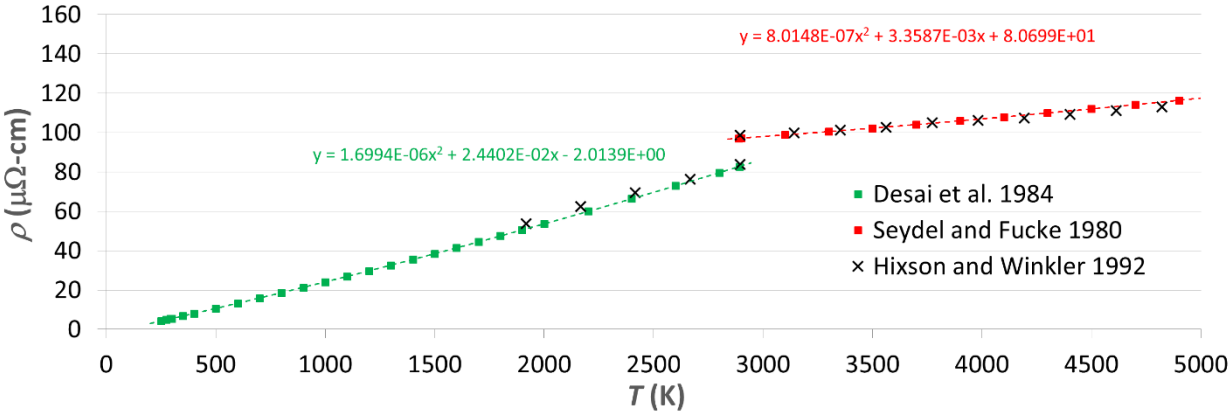

Fig. 14 Resistivity of pure Mo vs. temperature[22–24]

The dashed curves in Fig. 14 represent fits to second-order polynomials. The parameters that describe these polynomials are listed in Table 12.

Table 12 Parameters that describe polynomial fits to the curves in Fig. 14

Coefficient	Solid (298–2,896 K)	Liquid (2,896–4,952 K)
d	–2.0139E+00	8.0699E+01
e	2.4402E–02	3.3587E–03
f	1.6994E–06	8.0148E–07

6. Tungsten Wires

In this work, the melting point of W is taken to be 3,695 K, boiling point is 6,000 K, mass density is 19.25 g/cm^3, and atomic mass is 183.84.

6.1 Tungsten Heat Capacity

Unlike previous examples, the values used in this case are not the ones recommended by NIST. Here we use the values recommended in the extensive review of W thermophysical properties performed by Tolias et al.[15] As pointed out in Tolias et al., the values listed by NIST have not been reviewed since the 1960s, and better measurement methods have been developed since that time.

There is little information available about the gaseous phase of W due to its extremely high boiling point. Even its boiling point temperature is in doubt, with handbook values varying by nearly 200 K. Since this work is only meant to support simulations up to the point of boiling, the exact value is not important, and a value of 6,000 K is assumed. No heat capacity data for temperatures above 6,000 K were found, in any event.

In Tolias et al.[15] the recommended values for heat capacity and resistivity are reported as functions of temperature, with break points at 3,080 K and at the melting temperature (T_m = 3,695 K). Recommended values for heat capacity, which are plotted in Fig. 15, are derived from

$$C_p(T) = \begin{cases} 21.8684 + 8.0687 \times 10^{-3}T - 3.7562 \times 10^{-6}T^2 + 1.0759 \times 10^{-9}T^3 + 1.4066 \times 10^4/T^2 & 300 \le T \le 3080 \\ 2.022 + 1.315 \times 10^{-2}T & 3080 \le T \le 3695 \\ 51.3 & T \ge 3695 \end{cases} \quad (15)$$

where C_p is measured in J/(mol K) and T is measured in kelvin. When these functions are integrated and the specific heat of fusion is accounted for, the energies required to heat 1 g of W to various temperatures can be derived. These values are plotted in Fig. 16. As in Tolias et al., the heat of fusion is assumed to be 52.3 kJ/mol or 284.49 J/g.

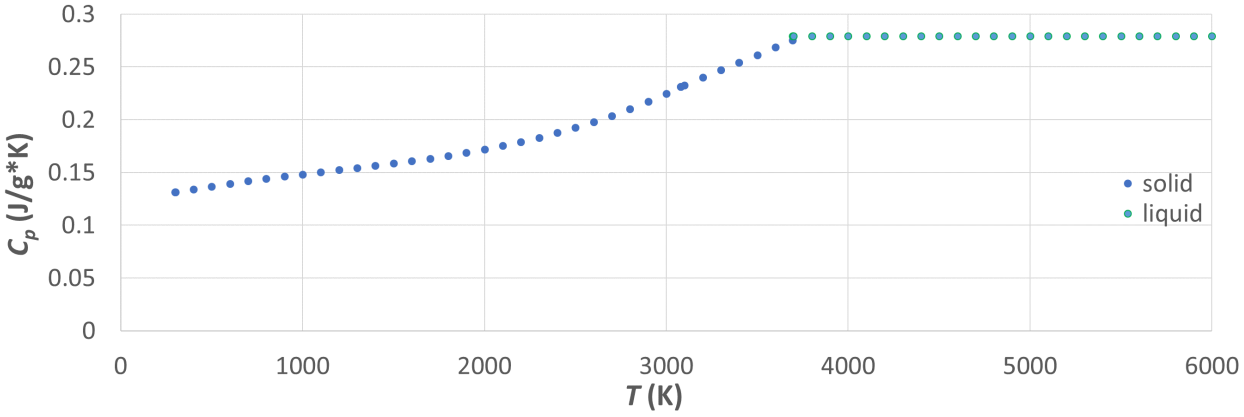

Fig. 15 Recommended values for the heat capacity of W[15]

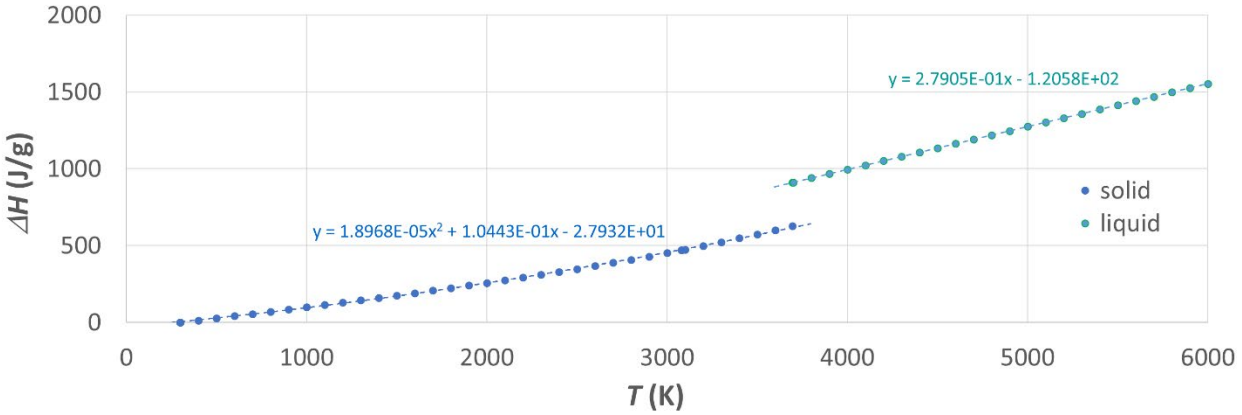

Fig. 16 Specific energy needed to raise W to various temperatures starting at room temperature

There is little agreement concerning the value of W's heat of vaporization. While not technically required for the simulations at hand, which are not accurate above the boiling point, the value assumed by the NIST WebBook,[11] 4,629.2 J/g, is assumed. This value falls roughly in the middle of the range of reported values.

The two dashed lines seen in Fig. 16 represent polynomial fits to intervals 298 ≤ T ≤ 3,695 K and 3,695 ≤ T ≤ 6,000 K, respectively. They represent functions of the form $\Delta H = a + b*T + c*T^2$, where ΔH is in joules per gram and T is in kelvin. These polynomial fits are used to develop a lookup table that yields temperature as a function of of energy input. The fitted coefficients used are listed in Table 13.

Table 13 Parameters that describe fits to the curves in Fig. 16

Coefficient	Solid (298–3,695 K)	Liquid (3,695–6,000 K)
a	–2.7932E+01	–1.2058E+02
b	1.0443E–01	2.7905E–01
c	1.8968E–05	…

6.2 Tungsten Resistivity

Tolias et al.[15] presented recommended values for W electrical resistivity in equation form:

$$\rho(T) = \begin{cases} -0.9680 + 1.9274 \times 10^{-2} T + 7.8260 \times 10^{-6} T^2 - 1.8517 \times 10^{-9} T^3 + 2.0790 \times 10^{-13} T^4 & 100 \le T \le 3695 \\ 135 - 1.855 \times 10^{-3} (T - T_m) + 4.420 \times 10^{-6} (T - T_m)^2 & 3695 \le T \le 6000 \end{cases} \quad (16)$$

where ρ is measured in μΩ-cm, T is measured in kelvin, and T_m is the melting point. These functions are plotted in Fig. 17.

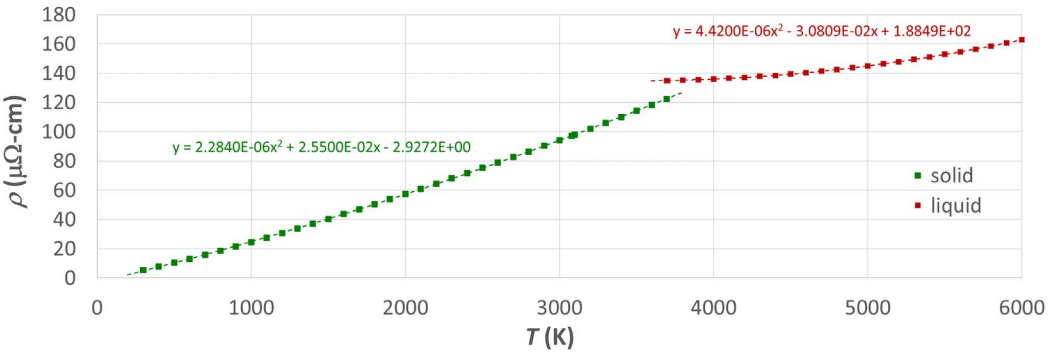

Fig. 17 Resistivity of pure W vs. temperature[15]

The dashed lines in Fig. 17 represent fits to quadratic polynomials of the form $\rho = d + e*T + f*T^2$, where ρ is resistivity in μΩ-cm and T is temperature in kelvin, for the purpose of developing a lookup table that yields resistivity as a function of temperature. The coefficients of these polynomials are listed in Table 14.

Table 14 Parameters that describe fits to the resistivity vs. temperature curves in Fig. 17

Coefficient	Solid (298–3,695 K)	Liquid (3,695–6,000 K)
d	–2.9272E+00	1.8849E+02
e	2.5500E–02	–3.0809E–02
f	2.2840E–06	4.4200E–06

7. Titanium Wires

In this work, the melting point of Ti is taken to be 1,939 K, boiling point is 3,631 K, mass density is 4.506 g/cm^3, and atomic mass is 47.867.

7.1 Titanium Heat Capacity

Titanium proves to be a more complicated case than other metals due to an allotropic phase transition (from the hcp α phase to the bcc β phase) that occurs at a temperature of around 890 °C. In this work, the onset temperature of the transition is assumed to be 1,152 K, as recommended by Kaschnitz and Reiter.[25]

The temperature range over which the phase transition occurs is assumed to be 30 K. Heat capacity numbers are derived from the NIST WebBook fits, as before. The published data used in those fits was last reviewed in 1979.[12,13]

The situation is further complicated by the fact that the α-phase data could not be satisfactorily fit by a single Shomate equation, so in that case the temperature ranges 298–700 K and 700–1,700 K were fit separately. Fitted Shomate equation parameters are listed in Table 15.

Table 15 Parameters that describe NIST's Shomate equation fits for pure Ti

Parameter	α phase (298–700 K)	α phase (700–1,700 K)	β phase (298–1,939 K)	Liquid phase (1,939–3,631 K	Gas phase (3,631–6,000 K)
A	2.26194E+01	4.43717E+01	2.30566E+01	4.72369E+01	9.27426E+00
B	1.89880E+01	–4.40923E+01	5.54133E+00	1.97519E–08	6.09211E+00
C	–1.81874E+01	3.17060E+01	–2.05588E+00	–5.33515E–09	5.77095E–01
D	7.08079E+00	5.22090E–02	1.61175E+00	4.90411E–10	–1.10364E–01
E	–1.43457E–01	3.61680E–02	–5.60750E–02	5.64855E–09	6.50441E+00
F	–7.92228E+00	–1.27201E+01	–4.33228E–01	–2.20527E+01	4.83009E+02
G	5.24096E+01	9.30877E+01	6.41269E+01	6.62022E+01	2.04157E+02
H	0.00000E+00	0.00000E+00	6.86000E+00	1.36520E+01	4.73629E+02

Figure 18 contains plots of C_p (in J/g*K) versus temperature based on the five fits described. Integrating these curves yields the specific energy needed to reach any given temperature, which is plotted in Fig. 19.

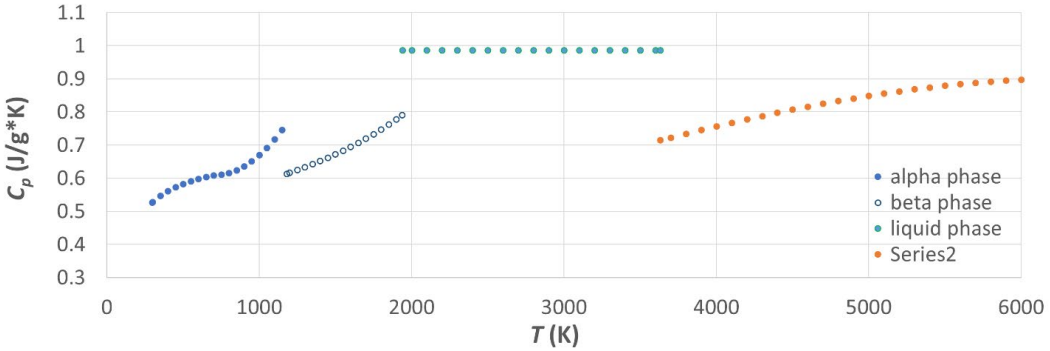

Fig. 18 Recommended values for the heat capacity of Ti[12,13]

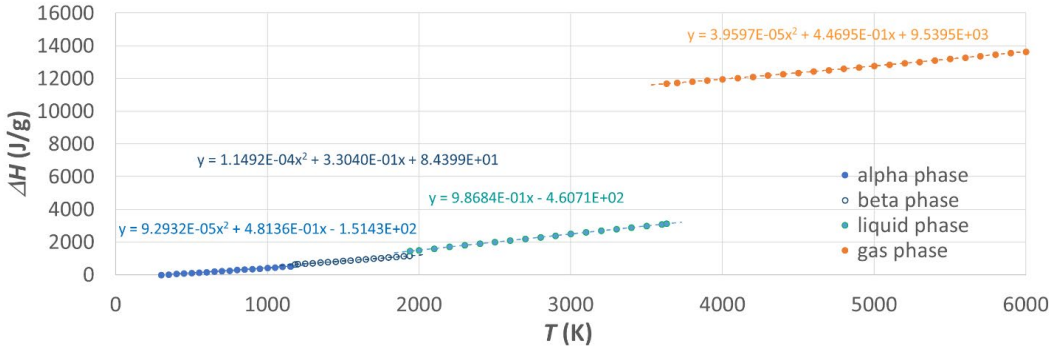

Fig. 19 Specific energy needed to raise Ti to various temperatures starting at room temperature

The dashed lines seen in Fig. 19 repesent polynomial fits to the temperature intervals corresponding to the α, β, liquid, and gaseous phases. They represent functions of the form $\Delta H = a + b*T + c*T^2$, where ΔH is in joules per gram and T is in kelvin. The fitted coefficients are listed in Table 16. Values within the phase

transition region (1,152–1,182 K) are generated by linear interpolation between the value at the end of the α phase fit and the beginning of the β phase fit.

Table 16 Parameters that describe fits to the energy vs. temperature curves in Figs. 19 and 20

Coefficient	α phase (298–1,152 K)	β phase (1,182–1,939 K)	Liquid phase (1,939–3,631 K)	Gaseous phase (3,631–6,000 K)
a	–1.5143E+02	8.4399E+01	–4.6071E+02	9.5395E+03
b	4.8136E–01	3.3040E–01	9.8684E–01	4.4695E–01
c	9.2932E–05	1.1492E–04	…	3.9597E–05

Figure 20 offers an expanded view of the alloptropic phase transition region in which the fitted curves seen in Fig 19 are compared with data from Kaschnitz and Reiter.[25]

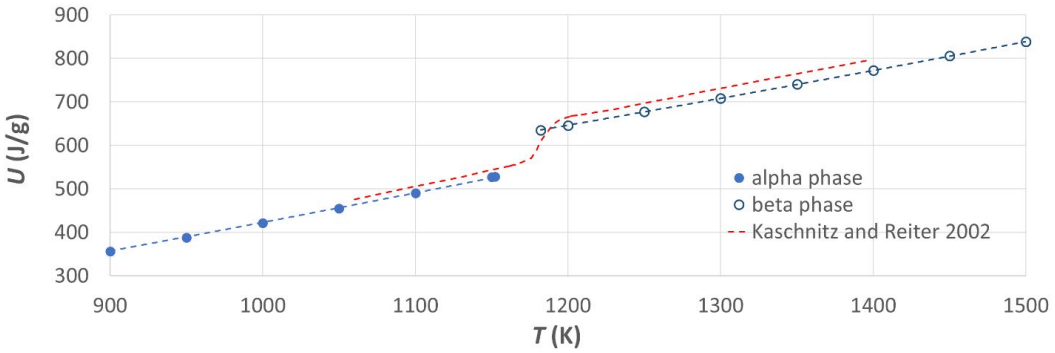

Fig. 20 Expanded view of the allotropic phase transition region seen in Fig. 19. Data from Kaschnitz and Reiter[25] are plotted for comparison.

As before, the polynomial fits in Fig. 19 were used to calculate key quantities to test the quality of the fits. Those quantities are listed in Table 17. The results based on the polynomial fits agree with the results based on the Shomate fits to within 0.3%.

Table 17 Key quantities derived from fits (Ti)

Quantity	From polynomial fits (J/g)	NIST Shomate (J/g)
Energy to heat from 298 to 1,939 K	1,156.8	1,157.8
Latent heat of fusion	295.8	295.0
Energy to heat from 1,939 to 3,631 K	1,669.6	1,669.7
Latent heat of vaporization	8,562.0	8,565.4

7.2 Titanium Resistivity

In a 2007 review of existing Ti resistivity data by Bel'skaya and Kulyamina,[26] it can be seen that there is little agreement between data sets. As a result, the authors

felt that they could not recommend specific values. After performing a statistical analysis, they concluded that the disagreement was largely due to varying levels of impurities in the samples studied.

In a prior review, Seydel and Fucke[24] recommended values for the resistivity of liquid Ti between the melting point and 5,000 K. The recommended values were presented as a function of temperature:

$$\rho(T) = 167.17 + 1.5890 \times 10^{-2}(T - T_m) + 6.7756 \times 10^{-7}(T - T_m)^2 \quad (17)$$

where ρ is given in μΩ·cm, T is temperature in kelvin, and T_m is the melting temperature.

Lacking universally accepted resistivity values for the alpha and beta phases, a decision was made to rely largely on values obtained in a single pulsed heating experiment performed by Gathers.[27] This was done primarily because the entire temperature range of interest was covered in this one experiment, and as such the values for the different phases would at least be consistent. Liquid-phase data from this experiment were also used, as they did not differ greatly from Seydel and Fucke's[24] recommended values.

Gathers' data posed some difficulty, however, as the resistivity data were plotted as a function of specific enthalpy ΔH (i.e., energy input per gram of material, starting at room temperature) rather than temperature. This is sometimes done in pulsed heating experiments because enthalpy (i.e., the amount of energy input into the system) is much easier to measure than temperature in such experiments.

In Gathers' work, the data are presented as a smoothed curve in a plot. Figure 21 contains a plot based on values extracted from Gathers' figure. Figure 22 contains the same data plotted as a function of temperature, where enthalpy was converted to temperature using the enthalpy versus temperature curves described.

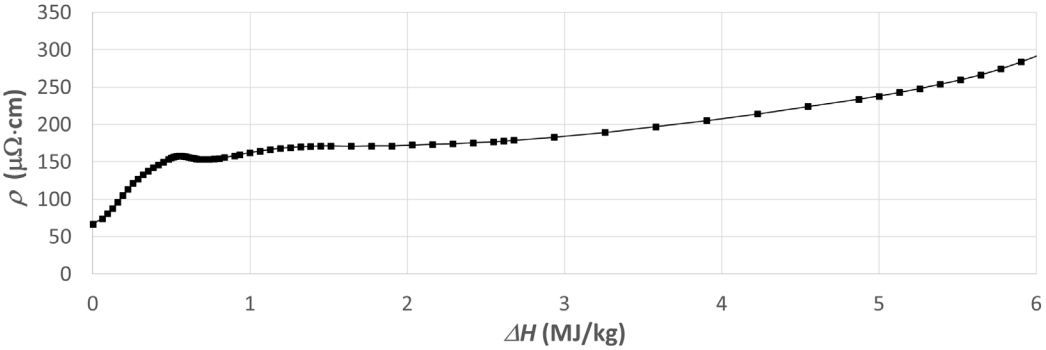

Fig. 21 Titanium resistivity vs. specific enthalpy relative to room temperature (derived from Fig. 1 in Gathers[27])

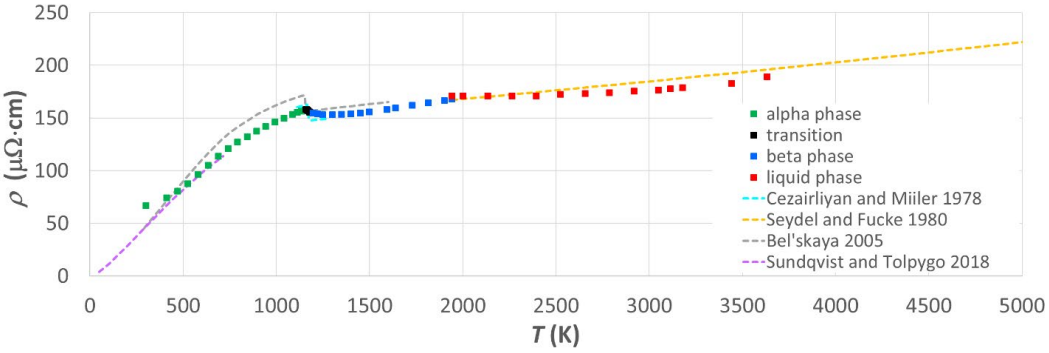

Fig. 22 Titanium resistivity vs. temperature data derived from Gathers[26] compared with others' data[24,28–30]

The liquid Ti resistivity values recommended by Seydel and Fucke[24] and the data from three other experimental studies[28–30] are all in reasonable agreement with Gathers' data.

Note that Bel'skaya[29] studied 99.7% pure Ti while Gathers[27] studied 99.9% pure Ti. Thus, it is no surprise that Bel'skaya's resistivity values are generally higher than Gathers' values. This does not explain the unusual behavior of Gathers' data near room temperature, however, where the values are higher than both Bel'skaya's[29] and Sundqvist and Tolpygo's[30] despite the fact that Sundqvist and Tolpygo also studied 99.9% pure Ti.

The other oddity in Gathers' data is that it lacks a sharp drop at the allotropic phase transition, as seen in both Bel'skaya's data[29] and in Cezairliyan and Miiler's data.[28] This may simply be due to overzealous smoothing on Gathers' part. While Cezairliyan and Miiler only studied a small temperature range around the allotropic phase transition, the low and high temperature extremities of their data set seem to align very well with Gathers' data set (Cezairliyan and Miiler also studied 99.9% pure Ti).

While not a major issue in the context of a simplified exploding-wire circuit model, it was nonetheless decided to remove the two discrepancies seen in Gathers' data by replacing key points near room temperature and near the allotropic phase transition with data from Sundqvist and Tolpygo[30] and Cezairliyan and Miiler,[28] respectively, prior to fitting. The results of the subsequent fits are referred to as "recommended values" in Fig. 23, where they are compared with Gathers' data, and again in Fig. 24, where they are compared with data from Cezairliyan and Miiler[28] and Sundqvist and Tolpygo.[30] Seydel and Fucke's[24] recommended values are also plotted.

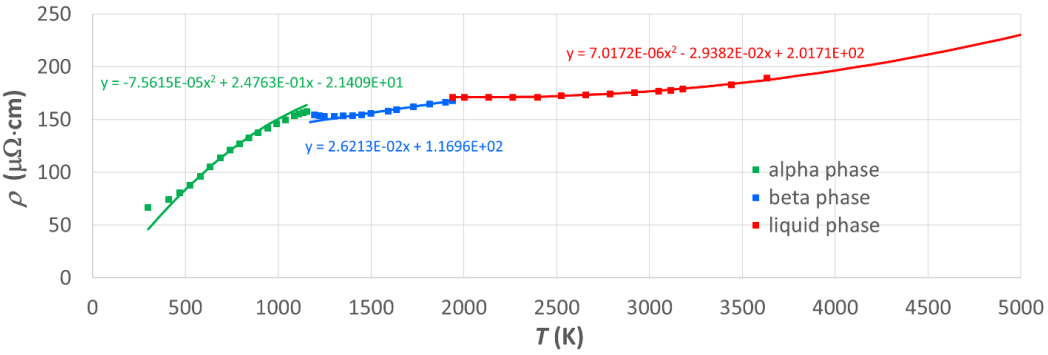

Fig. 23 "Recommended" Ti resistivity values (solid lines) compared with Gaithers'[27] data

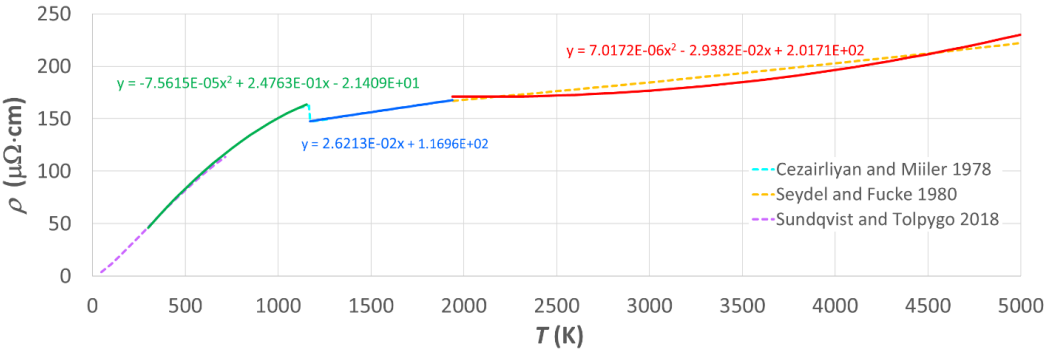

Fig. 24 "Recommended" Ti resistivity values (solid lines) compared with data from Seydel and Fucke,[24] Cezairliyan and Miiler,[28] Bel'skaya,[29] and Sundqvist and Tolpygo[30]

The recommended values plotted in Figs. 23 and 24 were fitted to polynomials of the form $\rho = d + e*T + f*T^2$, where ρ is resistivity in μΩ-cm and T is temperature in kelvin. The coefficients of these polynomials are listed in Table 18. Values covering the 1,152- to 1,182-K region are generated by linear interpolation between the endpoints of the α- and β-phase polynomial curves.

Table 18 Parameters that describe fits to the resistivity vs. temperature curves in Figs. 23 and 24

Coefficient	α phase (298–1,152 K)	β phase (1,182–1,939 K)	Liquid (1,939–3,631 K)
d	–2.1409E+01	1.1696E+02	2.0171E+02
e	2.4763E–01	2.6213E–02	–2.9382E–02
f	–7.5615E–05	0.0000E+00	7.0172E–06

8. Magnesium Wires

In this work, the melting point of Mg is taken to be 923 K, boiling point is 1,366 K, mass density is 1.738 g/cm^3, and atomic mass is 24.3050.

8.1 Magnesium Heat Capacity

Parameters for fits to Mg heat capacity data are listed in Table 19 of the NIST WebBook.[11] They yield C_p in J/mol*K and $H°$ in kJ/mol, as described in Eqs. 2 and 3. They are based on data last reviewed in 1983.[12,13]

Table 19 Parameters that describe NIST's Shomate equation fits for pure Mg

Parameter	Solid (298–923 K)	Liquid (923–1,366 K)	Gas (1,366–2,200 K)	Gas (2,200–6,000 K)
A	2.65408E+01	3.43090E+01	2.07731E+01	4.76085E+01
B	–1.53305E+00	–7.47103E–10	3.55920E–02	–1.54088E+01
C	8.06244E+00	6.14621E–10	–3.19170E–02	2.87597E+00
D	5.72170E–01	–1.59824E–10	9.10900E–03	–1.20806E–01
E	–1.74221E–01	–1.15201E–10	4.61000E–04	–2.70176E+01
F	–8.50160E+00	–5.43937E+00	1.40907E+02	9.74002E+01
G	6.39018E+01	7.59831E+01	1.73780E+02	1.77231E+02
H	0.00000E+00	4.79001E+00	1.47100E+02	1.47100E+02

Heat capacity values (in J/g·K) derived from these fits are plotted in Fig. 25. The energy needed to raise 1 g of Mg to various temperatures is plotted in Fig. 26.

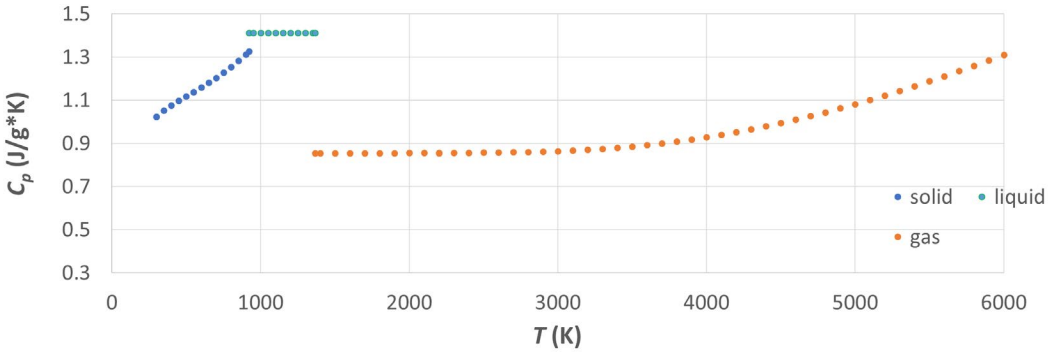

Fig. 25 Recommended values for the heat capacity of Mg[12,13]

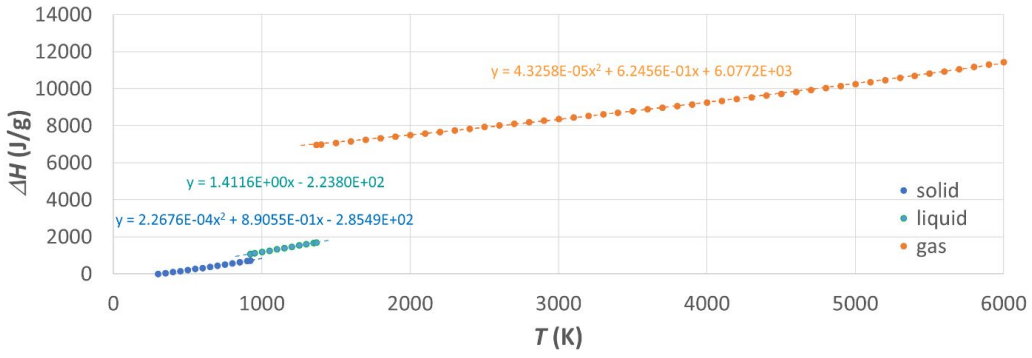

Fig. 26 Specific energy needed to raise Mg to various temperatures starting at room temperature

The dashed lines seen in Fig. 26 represent polynomial fits to the data. They represent functions of the form $\Delta H = a + b*T + c*T^2$, where ΔH is in joules per gram and T is in kelvin. The fitted coefficients are listed in Table 20.

Table 20 Parameters that describe fits to the energy per gram vs. temperature curves in Fig. 26.

Coefficient	Solid (298–923 K)	Liquid (923–1,366 K)	Gas (1,366–6,000 K)
a	–2.8549E+02	–2.2380E+02	6.0772E+03
b	8.9055E–01	1.4116E+00	6.2456E–01
c	2.2676E–04	…	4.3258E–05

Once again, key quantities were calculated using both the polynomial fits and the Shomate equation fits. These numbers are compared in Table 21. Agreement is within 0.8% in all cases.

Table 21 Key quantities derived from fits to Mg enthalpy curves

Quantity	From polynomial fits (J/g)	NIST Shomate (J/g)
Energy to heat from 298 to 1,358 K	729.64	728.91
Latent heat of fusion	349.47	348.79
Energy to heat from 1,358 to 2,843 K	625.34	626.75
Latent heat of vaporization	5,306.57	5,261.06

8.2 Magnesium Resistivity

Published data for the resistivity of Mg at elevated temperatures are difficult to find and generally quite dated. Most modern interest in Mg resistivity involves measurements made at cryogenic temperatures. Only one source of tabulated recommended values was found, in an ASM International (formerly the American Society of Metals [ASM]) handbook).[31] These values are plotted in Fig. 27.

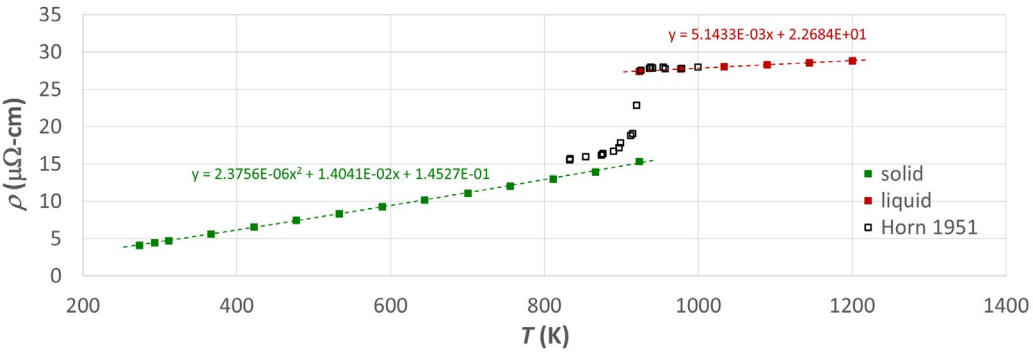

Fig. 27 Resistivity of pure Mg vs. temperature[25,28]

Unfortunately, the only reference quoted in that handbook is an internal Dow Chemical Company report from 1967,[32] so the sources of the reviewed data are unknown. That said, there is a figure in another ASM handbook[33] that appears to contain data identical to those seen in Fig. 27. That figure references six experiments, three from the 1950s and three from the 1930s. Data from one of those sources[33] are also plotted in Fig. 27. It appears to be in fair agreement with the ASM handbook values. As the data in Horn[34] are not corrected for thermal expansion, it is unlikely that the ASM handbook data are either. That is not an issue here, since the circuit model described here does not include the effects of thermal expansion in any event.

The dashed curves in Fig. 27 represent fits to first- or second-order polynomials. The parameters that describe these polynomials are listed in Table 22.

Table 22 Parameters that describe fits to the curves in Fig. 27

Coefficient	Solid (298–923 K)	Liquid (923–1,366 K)
d	1.4527E–01	2.2684E+01
e	1.4041E–02	5.1433E–03
f	2.3756E–06	…

9. Conclusion

We have developed an exploding-wire LRC circuit model that tracks temperature and phase changes in Cu, Al, Mo, W, Ti, and Mg wires. The model will primarily be used to plan exploding-wire experiments, as it can predict the extent of the heating process and timing of the phase changes. The ultimate purpose of the exploding-wire experiments will be to validate the ALEGRA code's material models. The circuit model described here can also be used to estimate the parasitic inductance and resistance in the circuit, both required inputs to the ALEGRA model.

The primary weakness of the circuit model is the assumption that the wire's geometry remains fixed throughout the heating event. Thus, the effects of thermal expansion are ignored and the model will tend to overestimate the inductance and resistance of the wire as its temperature increases. Future improvements to the model will include the effects of thermal expansion.

10. References

1. Robinson AC, Brunner T, Carroll S, Drake R, Garasi C, Gardiner T, Haill T, Hanshaw H, Hensinger D, Labreche D, et al. ALEGRA: an arbitrary Langrangian–Eulerian multimaterial, multiphysics code. AIAA Paper. 2008; p. 1196–1235. https://doi.org/10.2514/6.2008-1235.

2. Doney RL, Vunni GB, Niederhaus JH. Experiments and simulations of exploding aluminum wires: validation of ALEGRA-MHD. Aberdeen Proving Ground (MD): Army Research Laboratory (US); 2010 Sep. Report No.: ARL-TR-5299.

3. Tucker TJ, Toth RP. EBW1: a computer code for the prediction of the behavior of electrical circuits containing exploding wire elements. Albuquerque (NM): Sandia National Laboratories; 1975 Apr. Report No.: SAND-75-0041.

4. Valancius CJ, Garasi CJ, O'Malley PD. Power and energy of exploding wires. Albuquerque (NM): Sandia National Laboratories; 2017. Report No.: SAND2015-6351J.

5. Mao Z, Zou X, Wang X, Liu X, Jiang W. Circuit simulation of the behavior of exploding wires for nano-powder production. Laser and Particle Beams. 2009;27:49–55.

6. Knoepfel H. Pulsed high magnetic fields. Amsterdam (Holland): North Holland; 1970.

7. Hartmann W, Romheld M, Rohde K-D, Wabner A. Hydrodynamic instability of exploding wires. Proceedings of the 26th International Power Modulator Symposium and High-Voltage Workshop; 2004; p. 111–114.

8. Hollandsworth CE, Powell JD, Keele MJ, Hummer CR. Electrical conduction in exploded segmented wires. Journal of Applied Physics. 1998;84,(9):4992–5000.

9. Lehr J, Ron P. Foundations of pulsed power technology. Piscataway (NJ): IEEE Press; 2017.

10. Zellner MB, Doney R III, Uhlig WC, Berning P, Bartkowski P, Halsey S. Concept for spatial visualization of magnetic fields from exploding wires. Aberdeen Proving Ground (MD): CCDC Army Research Laboratory; 2019 Jun. Report No.: ARL-TR-8706.

11. National Institute of Standards and Technology. NIST WebBook. https://webbook.nist.gov.

12. Chase MW Jr. NIST-JANAF thermochemical tables. 4th edition, J Phys Chem Ref Data. 1998;1–1951. Monograph No.: 9.

13. Cox JD, Wagman DD, Medvedev VA. CODATA key values for thermodynamics. New York (NY): Hemisphere Publishing Corp.; 1984.

14. Gathers GR. Dynamic methods for investigating thermophysical properties of matter at very high temperatures and pressures. Rep Prog Phys. 1986;49:341–396.

15. Tolias P, EUROFusion MSTI Team. Analytical expressions for thermophysical properties of solid and liquid tungsten relevant for fusion applications. Nuclear Materials and Energy. 2017;13:42–57.

16. Grover FW. Inductance calculations. Mineola (NY): Dover Publications; 2004.

17. Matula RA. Electrical resistivity of copper, gold, palladium, and silver. J Phys Chem Ref Data. 1979;8(4):1147–1298.

18. Gathers GR. Thermophysical properties of liquid copper and aluminum. International Journal of Thermophysics. 1983;4(3):209–226.

19. D'esai PD, James HM, Ho CY. Electrical resistivity of aluminum and manganese. Journal of Physical and Chemical Reference Data. 1984;13:1131.

20. Brandt R, Neuer G. Electrical resistivity and thermal conductivity of pure aluminum and aluminum alloys up to and above the melting temperature. International Journal of Thermophysics. 2007;28(5):1429–1446.

21. Leitner M, Leitner T, Schmon A, Aziz K, Pottlacher G. Thermophysical properties of liquid aluminum. Metallurgical and Materials Transactions A. 2017;48A:3036–3045.

22. Hixson RS, Winkler MA. Thermophysical properties of molybdenum and rhenium. International Journal of Thermophysics. 1992;13(3):477–487.

23. Desai PD, Chu TK, James HM, Ho CY. Electrical resistivity of selected elements. Journal of Physical Chemistry Reference Data. 1984;13(4):1069–1096.

24. Seydel U, Fucke W. Electrical resistivity of liquid Ti, V, Mo and W. Journal of Physics F: Metal Physics. 1980;10:L203–L206.

25. Kaschnitz E, Reiter P. Enthalpy and temperature of the titanium alpha-beta phase transformation. International Journal of Thermophysics. 2002;23(5):1339–1345.

26. Bel'skaya EA, Kulyamina EY. Electrical resistivity of titanium in the temperature range from 290 to 1800K. High Temperature. 2007;45(6):785–796 (translated from Teplofizika Visokikh Temperatur. 2007;45(6):862–874).

27. Gathers GR. Electrical resistivity and thermal expansion of liquid titanium and zirconium. International Journal of Thermophysics. 1983;4(3):271–278.

28. Cezairliyan A, Miiler AP. Thermodynamic study of the $\alpha \rightarrow \beta$ phase transformation in titanium by a pulse heating method. Journal of Research of the National Bureau of Standards. 1978;83(2):127–132.

29. Bel'skaya EA. An experimental investigation of the electrical resistivity of titanium in the temperature range from 77 to 1600 K. High Temperature. 2005;43(4):546–543 (translated from Teplofizika Visokikh Temperatur. 2005;43(4):548–555).

30. Sundqvist B, Tolpygo VK. Saturation and pressure effects on the resistivity of titanium and two Ti-Al alloys. Journal of Physics and Chemistry of Solids. 2018;122:41–50.

31. Avedesian MM, Baker H. ASM specialty handbook, magnesium and magnesium alloys. Novelty (OH): ASM International; 1999.

32. Baker H. Physical properties of magnesium and magnesium alloys. Midland (MI): The Dow Chemical Company; 1967.

33. Buch A. Pure metals properties: a scientific and technical handbook. Novelty (OH): ASM International; 1999.

34. Horn FH. The change in electrical resistance of magnesium on melting. Phys Rev. 1951;84 (2): 855.

List of Symbols, Abbreviations, and Acronyms

1-D	one-dimensional
2-D	two-dimensional
Al	aluminum
ASM	American Society of Metals
Cu	copper
EBW	exploding bridge wire
LRC	inductance–resistance–capacitance
Mg	magnesium
MHD	magnetohydrodynamic
Mo	molybdenum
nH	nanohenrie
NIST	National Institute of Standards
Ti	titanium
W	tungsten

1 (PDF) DEFENSE TECHNICAL INFORMATION CTR DTIC OCA

1 (PDF) CCDC ARL FCDD RLD CL TECH LIB

20 (PDF) CCDC ARL FCDD RLW C P BARTKOWSKI FCDD RLW P R FRANCART FCDD RLW PA S BILYK J FLENIKEN T KOTTKE M MCNEIR C WOLFE P BERNING M COPPINGER W UHLIG L VANDERHOEF A VALENZUELA B WILMER J NESTA D MALONE FCDD RLW PD A BARD R DONEY G VUNNI M ZELLNER FCDD RLW PE P SWOBODA